NUMERICAL SIMULATION OF DEFLAGRATION-TO-DETONATION TRANSITION IN A PULSED DETONATION ENGINE

A. E. Zangiev[1], V. S. Ivanov[1,3], and S. M. Frolov[1,2,3]

[1]N. N. Semenov Federal Research Center for Chemical Physics
of the Russian Academy of Sciences
Moscow, Russia
[2]National Research Nuclear University MEPhI
Moscow, Russia
[3]Scientific Research Institute for System Analysis
Russian Academy of Sciences
Moscow, Russia

The air-breathing pulsed detonation engine (PDE) for an aircraft designed for a subsonic flight when operating on the products of pyrolysis of polypropylene was developed using the analytical estimates and parametric multivariant three-dimensional (3D) calculations. The PDE consists of an air intake with a check valve, a fuel supply system, a prechamber-jet ignition system, and a combustion chamber with an attached detonation tube. Parametric 3D calculations allowed choosing the best length of the PDE combustor, which provides an efficient mixing of air with fuel, the best way to ignite the mixture (prechamber-jet ignition), the best location of the prechamber, the minimum length of the section with turbulizing obstacles for flame acceleration and deflagration-to-detonation transition (DDT), and the best degree of filling the detonation tube with the fuel mixture to achieve the maximum completeness of combustion.

1 Introduction

In existing ramjets, a stationary operation process with continuous conversion of the chemical energy of fuel into the useful work of expanding products of deflagrative (subsonic) combustion is used. Continuous combustion of fuel in the combustor is ensured by special means and/or devices preventing flame blow-off and proceeds with a significant decrease in density (by a factor of 2 to 5) and with a slight decrease in pressure (by several percent) in the combustion products. Ramjets with pulsating (nonstationary) deflagrative combustion are often considered as an alternative to the ramjets with continuous deflagrative

DOI: 10.30826/NEPCAP2018-2-31

combustion of fuel. Such ramjets equipped with resonator tubes operate on the self-oscillating combustion of fuel with a significant decrease in density, but with a slight (by several percent) increase in pressure*. A well-known example is German V-1 vehicle of the Second World War.

Since 1940–1950s, thanks to the works of Ya. B. Zel'dovich [1] and B. V. Voitsekhovskii [2], a new idea arose that is the possibility of using detonative (supersonic) rather than deflagrative combustion of fuel in ramjets with the implication that the detonative combustion theoretically promises a significant increase in the energy efficiency. In contrast to stationary deflagrative combustion, in which the density and pressure of the products of chemical transformations decrease, in stationary detonative combustion, the density and pressure of reaction products increase substantially (density increases by a factor of 2, pressure increases by a factor of up to 15–17). Since stationary detonative combustion of fuel in an oblique detonation wave is accompanied by large entropy losses [1], the possibility of organizing detonative combustion in propagating detonation waves was considered: either in a continuous "spinning" detonation wave [2, 3] or in a pulse-periodic detonation wave [4]. Engines with continuous spinning detonation of fuel are called continuous-detonation engines (CDEs), and engines with pulse-periodic detonations are referred to as pulsed detonation engines. The combustion chamber in a CDE is made, as a rule, in the form of an annular chamber with axial air supply and with a distributed radial fuel supply by multiple jets. The spinning detonation wave continuously rotates in the annular gap downstream from the fuel jet holes, thus burning all the fuel entering the combustor during one turn of the wave around the engine axis, and the detonation products continuously expel into the ambient atmosphere through the nozzle, thus creating continuous thrust. The combustion chamber in the PDE is made, as a rule, in the form of a straight duct, periodically filled with fuel–air mixture and equipped with a mechanical check valve periodically blocking air access to the combustor. During the period when the valve is closed, a detonation wave runs along the duct, thus burning all the fuel accumulated in the combustor, and the detonation products expel into the ambient atmosphere through the nozzle, creating a pulse of thrust.

This paper is a continuation of the studies described in [5]. In [5], firing tests of the PDE model with a mechanical check valve were conducted in a subsonic wind tunnel with a free air jet of the Mach number ranging from 0.65 to 0.85. Liquid propane was used as a fuel. Operating modes with a frequency of up to 10 Hz, an average thrust of up to 30 N, and an average specific impulse of up to 1000 s were obtained. Note that according to the one-dimensional (1D) analysis [6, 7], the PDE of [5] could exhibit the specific impulse on the level of 2000 s. The difference in the measured and estimated values (1000 and

*The latter does not contradict the laws of conservation of mass and momentum, since the operation process in such an engine is nonstationary.

2000 s) is probably due to the differences in the PDE operation. Thus, in the experiments of [5], the PDE operated based on the DDT phenomenon, when a large part of the tube length was used for flame acceleration. On the contrary, the idealized PDE performance in [6, 7] is calculated with direct detonation initiation.

The purpose of our further research is the development, based on the results of [5], of a PDE operating on the products of pyrolysis of solid fuel like polypropylene. The possibility of using the products of pyrolysis of solid combustible in ramjets operating on detonation combustion was considered in [8] where granular polypropylene was selected as a solid fuel. In [8], a gas generator was designed, manufactured, and tested to obtain polypropylene pyrolysis products at a decomposition temperature of 650 to 800 °C. Chromatographic analysis of the products showed that they mainly consist of propylene C_3H_6, isobutene iso-C_4H_8, ethane C_2H_6, methane CH_4, ethylene C_2H_4, and propane C_3H_8. Experiments on the DDT in air mixtures of hot polypropylene pyrolysis products were carried out. It was shown that in mixtures with air, enriched in fuel (with an air-to-fuel equivalence ratio ranging from 0.73 to 0.90), at normal pressure and elevated initial temperature (70–90 °C), the pyrolysis products of polypropylene have detonability somewhat similar or even better than the detonability of liquefied petroleum gas (LPG) in a stoichiometric mixture with air under normal conditions. This means that the polypropylene pyrolysis products can be readily modeled by the stoichiometric LPG–air mixture.

There are several publications in the open literature relevant to experimental studies of hydrocarbon-fueled air-breathing PDEs, the subject of this paper. Brophy *et al.* [9, 10] investigated detonability limits of JP-10–air aerosol in a pulse detonation combustor which utilizes a JP-10–oxygen predetonator unit as the source of direct detonation initiation. The results obtained indicate that for a JP-10–air aerosol to successfully detonate at a detonation velocity of ~ 1800 m/s, a Sauter Mean Diameter of aerosol droplets below approximately 3 μm is required and/or a large fraction of fuel vapor must be present. Schauer *et al.* [11] investigated DDT in a PDE fueled by air mixtures of propane, octane, low-lead aviation gasoline, jet fuel JP-8, and the high energy-density jet fuel JP-10. Frolov and Aksenov [12] obtained DDT in a continuous flow of a mixture of partially prevaporized TS-1 jet kerosene with air at atmospheric pressure and a tube wall temperature of 110–130 °C. In the thermostated tube 52 mm in diameter consisting of a kerosene prevaporizer, a straight section with a Shchelkin spiral, and a smooth-walled tube coil, DDT occurred at a distance of about 2 m in 5–6 ms at a low ignition energy of 5 J. The registered values of the detonation velocity were 1700–1800 m/s. Huang *et al.* [13, 14] reported the experimental studies of DDT in kerosene–air mixture in a 1-meter-long and 29-millimeter-diameter PDE with the aerovalve and two different obstacle configurations in the detonation tube. The initial temperature of incoming air was 25 °C and the temperature of preheated kerosene was 110 °C. The registered velocities of periodic reaction

fronts were as low as 1200–1300 m/s. Recently, Jiun-Ming Li *et al.* [15] discovered experimentally that a Jet-A/air PDE can operate in a relatively cold environment when an excessively fuel-rich mixture is used. The experimental results and theoretical phase equilibrium calculations showed that the vapor-phase equivalence ratio is vital for successful detonation initiation of spray detonations via a DDT process.

The existing theoretical models of the two-phase detonation are not satisfactory: they consider the average flow behind the lead shock wave [16–25]. Interactions between drops and gas are most often described using various empirical correlations obtained for a single spherical particle in the steady-state gas flow. Drop vaporization is usually modeled by the well-known d^2-law disregarding the transient heating period of a drop which can occupy the major part of drop lifetime, as well as drop deformation and internal liquid circulation [26]. The convective enhancement of heat and mass transfer in the two-phase flow with highly unsteady velocity slip between phases is modeled by empirical corrections like Ranz–Marshall relationship [27] obtained for a wetted porous sphere at steady-state flow conditions. The aerodynamic breakup of drops behind detonation fronts is modeled based on empirical correlations for drop behavior behind idealized planar incident shock waves in inert gas [28] neglecting the influence of both the inhomogeneous structure of the lead detonation front and upstream-propagating secondary pressure waves originating in the subsonic reaction zone of a two-phase detonation. The momentum exchange between phases is usually modeled using a concept of the quasi-steady-state aerodynamic drag coefficient for a single spherical particle, thus omitting the effects of drop deformation, neighbor-particle wakes, etc. When modeling chemical energy release, it is often assumed that the heat release rate is ultimately controlled either by drop vaporization (fine drops) or by aerodynamic drop breakup (large drops). Such models of two-phase detonations do not account for finite rates of chemical reactions and fail to predict detonability limits. In some cases, either empirical correlations for ignition delays [21] or detailed fuel oxidation mechanisms [29, 30] are applied to describe the detonation structure based on the average temperature and gas-phase composition, thus ignoring high intrinsic sensitivity of chemical transformations to local mixture temperature and composition. Finally, in all available models, the screening effects of neighbor drops on interphase mass, momentum, and energy fluxes are modeled indirectly, through instantaneously-changing averaged values of gas flow parameters. As a result, the finite rates of accompanying physical and chemical phenomena are completely neglected. The 1D theory of steady-state two-phase detonation reported in [25] can predict the influence of fuel type, active additives, pressure, gas and liquid temperature, as well as the liquid prevaporization degree on the detonability limits and detonation structure due to the resolution of local physical and chemical phenomena, including finite-rate multistep ignition and combustion chemistry and group-screening effects of drops in suspensions. However,

this theory has not yet been extended to time-dependent multidimensional formulation.

In view of the drawbacks of the existing theoretical models of two-phase detonations, the best what could be currently expected from the multidimensional calculations of DDT in two-phase LPG–air mixtures are the trends in the variation of the DDT run-up distance under the effect of different governing parameters. Knowing these trends, one could try to optimize the design of the PDE. In this paper, we have used the computational fluid dynamics (CFD) approach reported in [31] to design the PDE.

2 Assessment of Integral Performance

Figure 1 shows a schematic diagram of the PDE. The PDE is a straight channel with specified cross-sectional area and length. It consists of an air intake combined with a check valve, a fuel supply system, an ignition system, a combustor where fuel is mixed with air and ignited, a detonation tube, and an outlet device (nozzle). The detonation tube consists of the flame acceleration section with turbulizing obstacles in the form of orifice plates. The blockage ratio and spacing of the orifice plates varies along the tube to ensure fast DDT [32]. Currently, the operation frequency of the PDE is limited by the response time of the mechanical check valve: the maximum frequency is ~ 20 Hz [5]. The operation cycle includes filling the combustor and the detonation tube with the fuel–air mixture while the check valve is open, then igniting the mixture, closing the check valve (actively or passively), DDT, burning the fuel–air mixture in the propagating detonation wave, and expelling the detonation products through the nozzle into the ambient atmosphere. At the stages of combustion of fuel–air mixture and the expelling of detonation products through the nozzle, a static overpressure is maintained on the inner surface of the closed check valve, which creates the force acting against the approaching air flow, the thrust force. When the static pressure at the check valve drops to the level of the total pressure of the approaching air flow, the check valve is opened and the operation cycle of the PDE repeats.

The base fuel for the PDE is LPG.

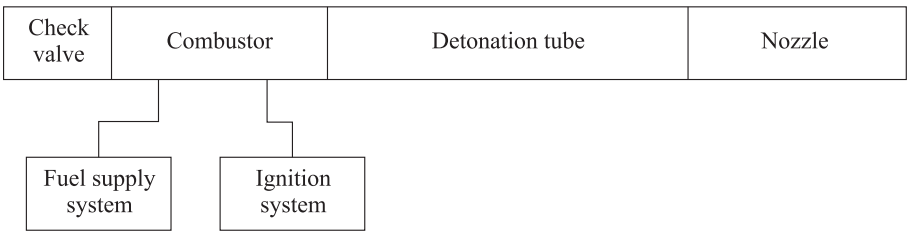

Figure 1 Schematic diagram of the PDE

To estimate analytically the expected integral performance of the PDE (operation frequency f, full thrust T, effective thrust F, and aerodynamic drag R), calculations were made for a PDE of length L ranging from 1 to 3 m with a square cross section of 100×100 mm (corresponding to a cross section of a round tube of 113 mm in diameter) at different flight speeds. A scheme of the PDE without an exit nozzle was considered. Calculations are based on the following formulae:

$$f = \frac{VC_{\text{in}}}{L};$$
$$T = \dot{m}_f I_{\text{sp}} g;$$
$$F = T + R;$$
$$R = -\frac{C_X S \rho V^2}{2};$$
$$\dot{m}_f = \rho V S Y_{\text{st}} C_{\text{in}} C_f$$

where V is the flight speed; I_{sp} is the fuel-based specific impulse; g is the acceleration of gravity; ρ is the air density; S is the cross-sectional area of the PDE; $\dot{m}_f$ is the fuel consumption; C_X is the aerodynamic drag coefficient of the PDE; Y_{st} is the fuel mass fraction in the stoichiometric LPG–air mixture; C_{in} is the discharge coefficient of the PDE; and C_f is the fuel fill factor of the PDE. Forces T, F, and R are treated as positive if they are directed opposite to the approaching air flow.

The calculations are based on the following values of the governing parameters and coefficients: $I_{sp} = 1000$ s (obtained experimentally in [5]); $C_X = 1.0$; $Y_{\text{st}} = 0.06$; $C_{\text{in}} = 0.5$ (i. e., 50% of the approaching air flow enters the intake,

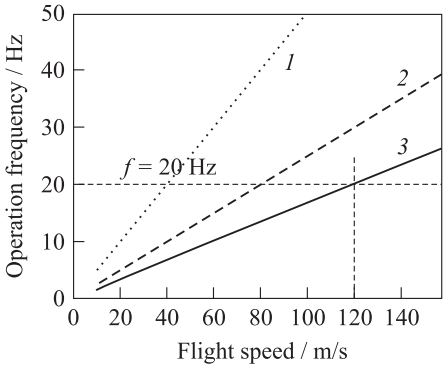

Figure 2 Calculated dependencies of the operation frequency on the flight speed for the PDE of different lengths: *1* — $L = 1$ m; *2* — 2; and *3* — $L = 3$ m

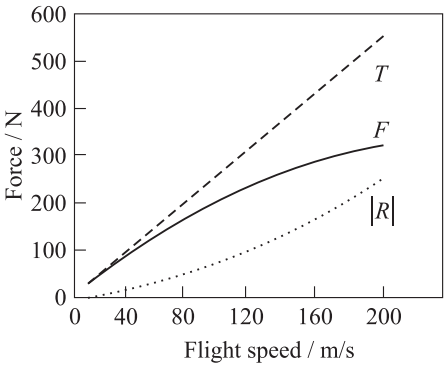

Figure 3 Calculated thrust parameters vs. flight speed for a 3-meter long PDE with 100×100 mm cross-sectional area

the losses are due to the presence of baffles in the design of the check valve and with the pressure loss associated with air purging through the engine path); and $C_f = 0.8$ (i. e., the detonation tube is filled with the fuel–air mixture during 80% of the cycle time, whereas the remaining 20% of the cycle time are used for the mixture to burn out and the detonation products to expel from the engine).

Figures 2 and 3 show the results of calculations in the form of the $f(V)$ curves at $L = 1$, 2, and 3 m (Fig. 2) and in the form of dependencies $T(V)$, $F(V)$, and $R(V)$ at $L = 3$ m (Fig. 3). In view of the current limitations imposed on the check valve in terms of the maximum operation frequency (20 Hz), there is a limiting flight speed at which the maximum effective thrust of the PDE can be attained: in the 3-meter long PDE, it is possible to realize an operation process at a flight speed of up to 120 m/s (see Fig. 2) with an effective thrust at the sea level up to 250 N (see Fig. 3). In the 2-meter long PDE, the maximum speed of flight at the same operating frequency is 80 m/s.

3 Computational Fluid Dymanics Approach

The design of the PDE was created using multivariant numerical calculations applying a technique described, e. g., in [31].

The operation process in the PDE was simulated in the 3D approximation. The underlying mathematical model is based on the two-phase Eulerian–Lagrangian approach with the two-way coupling between the phases. The gas phase is treated within the Eulerian formalism, whereas the liquid fuel phase is considered within the Lagrangian parcel approach.

The governing equations for the gas phase are the Unsteady Reynolds-Averaged Navier–Stokes (URANS) equations of conservation of mass, momentum, and energy for a nonstationary compressible turbulent reacting flow with the source terms describing interphase interactions. The gas-phase turbulent fluxes of mass, momentum, and energy were simulated using the k–ε model of turbulence (k is the kinetic energy of turbulence and ε is its dissipation).

The liquid phase is represented by multiple dispersed parcels each containing N identical droplets of diameter d. The motion of each parcel is described by the motion of a single droplet in it according to the equations of motion:

$$\frac{dx_{kd}}{dt} = u_{kd}\,; \quad m_d \frac{du_{kd}}{dt} = F_k$$

where index d denotes the droplet properties; x_{kd} is the cartesian coordinate of a droplet ($k = 1, 2, 3$); u_{kd} is the kth component of the parcel velocity; m_d is the single droplet mass; and $F_k = F_{kf} + F_{kg} + F_{kp}$ is the kth components of the force acting on a single droplet, which is composed of the aerodynamic drag F_{kf}, gravity F_{kg}, and pressure F_{kp} forces. The forces are calculated using the following relationships:

$$F_{kf} = \frac{1}{2}\rho A_d C_d U_k |U| ;$$
$$F_{kg} = (\rho_d - \rho) V_d g_k ;$$
$$F_{kp} = V_d \nabla P_k$$

where A_d is the droplet midsection area; C_d is the aerodynamic drag coefficient; V_d is the droplet volume; g_k is the kth component of the acceleration of gravity; ∇P_k is the kth component of the pressure gradient vector; and U_k is the relative velocity of phases defined as

$$U_k = \overline{u_k} + u'_k - u_{kd} .$$

The drag coefficient C_d is determined based on the value of the relative Reynolds number $\mathrm{Re} = \rho|U|d/\mu$ based on the length of the relative velocity vector, $|U|$:

$$C_d = \begin{cases} \dfrac{24}{\mathrm{Re}_d}\left(1 + 0.15\mathrm{Re}^{0.687}\right) , & \mathrm{Re} < 10^3 ; \\ 0.44 , & \mathrm{Re} \geqslant 10^3 . \end{cases}$$

It is assumed that during motion, the droplets undergo aerodynamic breakup once its Weber number $\mathrm{We} = d\rho U^2/\sigma$ exceeds the critical value: $\mathrm{We} > \mathrm{We}_c \approx 12$. Here, σ is the liquid surface tension. The breakup phenomenon is described by the WAVE model [32], claiming that during the characteristic breakup time τ_b, the droplet radius $r = d/2$ continuously decreases to a certain "stable" value r_s:

$$\frac{dr}{dt} = -\frac{r - r_s}{\tau_b} .$$

The "stable" radius of the droplet is determined as

$$r_s = \begin{cases} b_0\lambda & \text{at } b_0\lambda < r ; \\ \min\left[\left(\dfrac{3\pi r^2|U|}{2\Omega}\right)^{1/3}, \left(\dfrac{3r^2\lambda}{4}\right)^{1/3}\right] & \text{at } b_0\lambda > r \end{cases}$$

where λ is the perturbation wavelength; Ω is the rate of perturbation growth; and $b_0 = 0.61$ is the model constant. The characteristic time τ_b is given by the relationship:

$$\tau_b = b_1 \frac{r}{|U|}\sqrt{\frac{\rho_d}{\rho}}$$

where b_1 is the model parameter varying from 10 to 30.

For determining the source terms in the mass and energy conservation equations for the gas phase, the Dukowicz model [33] of droplet heating and evaporation is used. The mass and energy conservation equations for a single droplet in parcel read:

$$\frac{dm_d}{dt} = \frac{\dot{Q}\dot{f}_{vs}}{\dot{q}_s};$$
$$m_d c_d \frac{dT_d}{dt} = \dot{Q} + L\frac{dm_d}{dt}$$

where $\dot{Q}$ is the heat flux to the droplet; c_d is the liquid specific heat; L is the latent heat of vaporization; $\dot{f}_{vs}$ and $\dot{q}_s$ are the specific (per unit surface of the droplet) heat and mass fluxes; and indices s and v denote surface and vapor, respectively.

The unknown fluxes are determined using the following relationships:

$$\dot{Q} = \pi\kappa d\mathrm{Nu}\,(T - T_d)\,, \qquad \mathrm{Nu} = 2 + \mathrm{Re}^{1/2}\mathrm{Pr}^{1/3}\,;$$
$$\frac{\dot{f}_{vs}}{\dot{q}_s} = -\frac{B_Y}{h - h_s - (h_{vs} - h_s)(Y_v - Y_{vs})}\,, \quad B_Y = \frac{Y_{vs} - Y_v}{1 - Y_{vs}}$$

where κ is the gas thermal conductivity; and Nu and Pr are the Nusselt and Prandtl numbers. Note that all thermophysical parameters of gaseous species on the droplet surface are determined based on the assumption of phase equilibrium.

To couple mass, momentum, and energy variations in the liquid phase with those in the gas phase, the force F_i, as well as mass $\dot{Q}\dot{f}_{vs}/\dot{q}_s$ and heat $\dot{Q}$ fluxes calculated for a single droplet in the parcel are then taken with the opposite sign, multiplied by N and entered as a source term in the equations of mass, momentum, and energy conservation for the gas-phase. The same procedure is used for other parcels available in the given location at a given time.

Simulation of chemical sources during turbulent combustion and DDT includes the contributions of both frontal combustion and volumetric preflame reactions. For their determination, the Flame Tracking algorithm for the explicit tracking of the flame front is used, and the contributions of the volumetric reactions are determined using the Particle method. The coupled Flame Tracking–Particle (FTP) algorithm is supplemented with the database of tabulated laminar flame velocities for propane–air mixtures in the wide range of initial temperature, pressure, and fuel-to-air equivalence ratio Φ as well as the reaction kinetics of preflame fuel oxidation. Table 1 shows the fragment of the database of laminar flame velocities for propane–air mixtures of different compositions [34, 35]. Tables 2 and 3 show the overall reaction mechanism of propane oxidation with the special treatment of low-temperature ($T < T_*$) and high-temperature ($T \geqslant T_*$) oxidation where T_* is the transition temperature (775 K). The rate-limiting reaction #1 in Table 1 is conditionally treated as bimolecular. The rate constant of the ith reaction is defined as $k_i = A_i T^{n_i} \exp(E_i/(RT))$ where A_i is the preexponential factor depending on pressure P; n_i is the temperature exponent; E_i is the activation energy; and R is the gas constant. The value of the transition temperature T_* has been found based on the best fit between the calculations using the overall mechanism of Tables 2 and 3 and the detailed reaction mechanism [36].

Table 1 Laminar flame velocities for propane–air mixtures of different composition at different temperatures ($P = 1$ atm) [35]

T_0, K	Φ						
	0.5	0.6	0.8	1,0	1.2	1.5	2.0
293	—	13	32	39	36	21	10
450	—	30	66	78	73	42	18
600	36	66	125	143	132	77	25
680	54	99	181	198	181	103	30
750	75	132	234	247	222	131	35
820	90	187	330	333	296	166	40
900	140	266	470	451	392	216	50

Table 2 Overall kinetic mechanism of gas-phase oxidation of propane [34, 35], P is taken in atm

No.	Reaction	H, kcal/mol	A_k, mol, l, s	n_k	E_k, kcal/mol
1	$C_3H_8 + 3.5O_2 \to 3CO + 4H_2O$	290	$\dfrac{A_1}{P}$	0	E_1
2	$CO + H_2O \to CO_2 + H_2$	10	$\dfrac{10^{12}}{P}$	0	41.5
3	$CO_2 + H_2 \to CO + H_2O$	10	$3.1\dfrac{10^{13}}{P}$	0	49.1
4	$H_2 + H_2 + O_2 \to H_2O + H_2O$	114	$7\dfrac{10^{13}}{P^{0.5}}$	0	21
5	$CO + CO + O_2 \to CO_2 + CO_2$	134	$8.5\dfrac{10^{12}}{P^{1.5}}$	0	21

Table 3 Arrhenius parameters of reaction # 1 in Table 2 ($P = 1$ atm [34, 35])

$T < T_*$			T_*, K	$T \geqslant T_*$		
A_1, l/(mol·s)	n_1	E_1, kcal/mol	775	A_1, l/(mol·s)	n_1	E_1, kcal/mol
$1.96 \cdot 10^{12} P$	0	40		$1.73 \cdot 10^{12} P^{0.23}$	0	45

The set of governing equations supplemented by the k–ε-model of turbulence and the conjugate FTP algorithm was closed by the caloric and thermal equations of state of an ideal gas with variable specific heats as well as by initial and boundary conditions. All thermophysical parameters of the gas and liquid were considered variable. For a numerical solution, we used a method based on the finite-volume discretization of the equations with the first order of approximation

in space and in time. To avoid excessive mesh refinement near solid surfaces, the standard wall functions were used. The baseline computational mesh consisted of 800,000 cells. The nominal number of notional particles in each computational cell was 20. To decrease the computational time, the Particle algorithm was activated upon ignition. The effect of the dimensions of the computational cells on the flow structure was checked by additional calculations on essentially smaller meshes. Some examples of numerical solutions for the homogeneous mixtures can be found in [31, 37].

4 Design of the Thrust Module

Calculations were performed for the conditions when the PDE is placed in a free air stream with the approaching flow velocity of 10 m/s with the injection of LPG into the combustor. As a result of the calculations, a 3-meter long PDE with a square-circular cross section is designed (Fig. 4*a*): the intake with a check valve and combustor have a square section of 100×100 mm and the detonation tube is made in the form of a round tube with a diameter of 100 mm equipped with turbulizing obstacles. The exit nozzle is absent.

The check valve (Fig. 4*b*) contains petals freely rotating with their axes between the casing and grid, thus opening and closing the access of air to the combustor due to arising pressure difference. To reduce the stroke of the petals, the grid of the check valve is positioned at an angle of 45° to the approaching air flow.

The turbulizing obstacles are the 2-millimeter thick orifice plates with the blockage ratio varying from 50% to 20%. They are installed in the detonation tube with a variable pitch equal to 40 mm near the combustion chamber and 80 mm in the region of DDT. The total length of the obstructed part of the

(*a*)

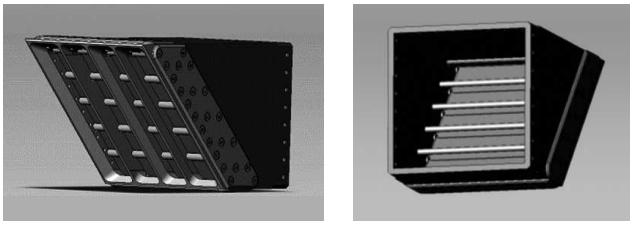

(*b*)

Figure 4 The 3D model of PDE (*a*) and the views of the check valve from outside and inside (*b*)

detonation tube is 2 m. The blockage ratio and the pitch of the orifice plates were chosen in such a way as to provide DDT at the minimum distance according to the fast DDT concept described in [38]. The concept of [38] consists in the careful selection of the shape and placement of turbulizing obstacles, so as to provide an optimum balance between the rates of flame acceleration and shock wave amplification.

The specified parameters of the PDE are close to the parameters adopted in the analytical estimates of section 2.

With the help of parametric 3D calculations, the best length of the combustor is selected which ensures efficient mixing of fuel with air. Also, the best method of ignition (prechamber-jet ignition), the best location of the prechamber, the best arrangement of the turbulizing obstacles in the tube to obtain the minimum length of the section of flame acceleration and DDT, and the best degree of filling the detonation tube with the fuel–air mixture for achieving the maximum completeness of combustion are determined. The design and operation mode of the PDE for attaining the minimum pressure loss and the maximum thrust were not optimized.

As an example of calculation, Fig. 5 shows the calculated field of fuel vapor mass fraction in the inner path of the PDE at the end of the stage of filling the detonation tube with the fuel–air mixture. The liquid fuel is seen to be injected from the step in the upper wall of the PDE and hit the bottom wall. The initial diameter of droplets in the injector nozzle is taken equal to 100 μm. The secondary aerodynamic droplet breakup in the approaching air stream results in the formation of droplets with a diameter of about 20 μm. In the prechamber and its surroundings, the fuel mixture is seen to be enriched with fuel, whereas in the detonation tube, the composition of the fuel–air mixture is close to stoichiometric

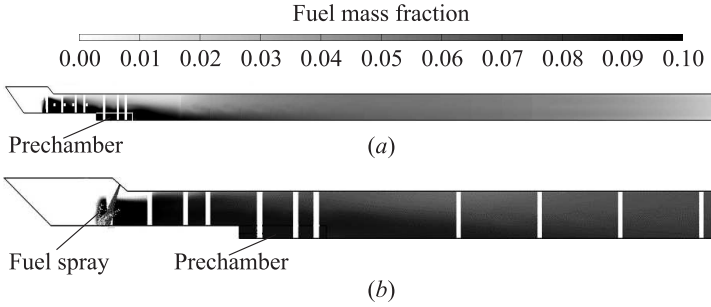

Figure 5 An example of the calculated field of fuel vapor mass fraction in the inner path of the PDE at the end of the filling stage of the detonation tube with a combustible mixture (check valve is open) (*a*); and the exploded view of the initial part of the PDE with the fuel spray (*b*)

(≈ 6%). At the end of the detonation tube, the fuel–air mixture is seen to be fuel-lean due to incomplete filling and due to admixing of the purging air which separates the fresh reacting mixture from the combustion products of the previous cycle.

Another example of calculation is shown in Fig. 6 in the form of the calculated temperature fields in the inner path of the PDE at different time instants after the ignition of the fuel–air mixture. The ignition was simulated by placing a hot flame kernel with a diameter of 3 mm behind the ledge of the prechamber. In this example, the DDT is reached at the end of the last section of the detonation tube with the turbulizing obstacles at about 9 ms after ignition. The

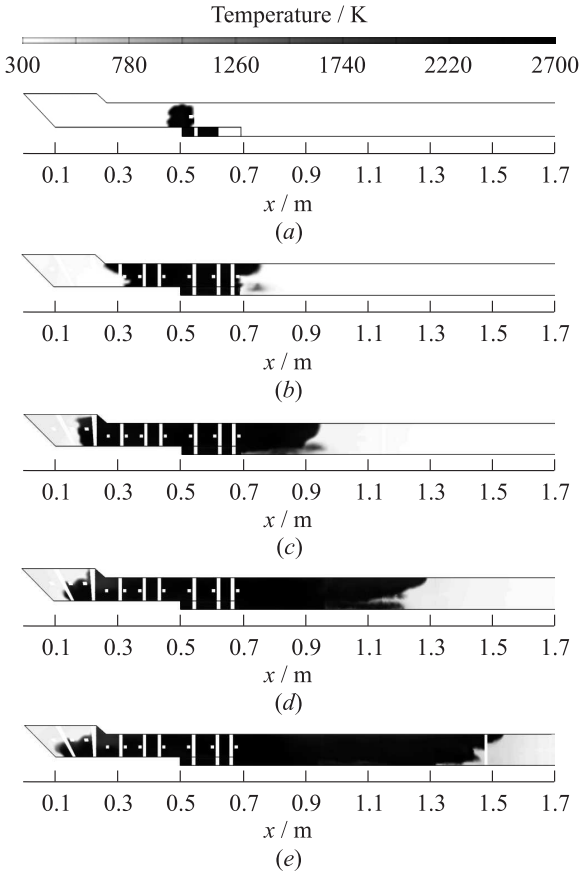

Figure 6 The calculated gas temperature field in the middle longitudinal section of the inner path of the PDE path at different time instants after prechamber ignition (check valve is closed): (*a*) 3 ms; (*b*) 5; (*c*) 6; (*d*) 7; and (*e*) 7.5 ms (*to be continued*)

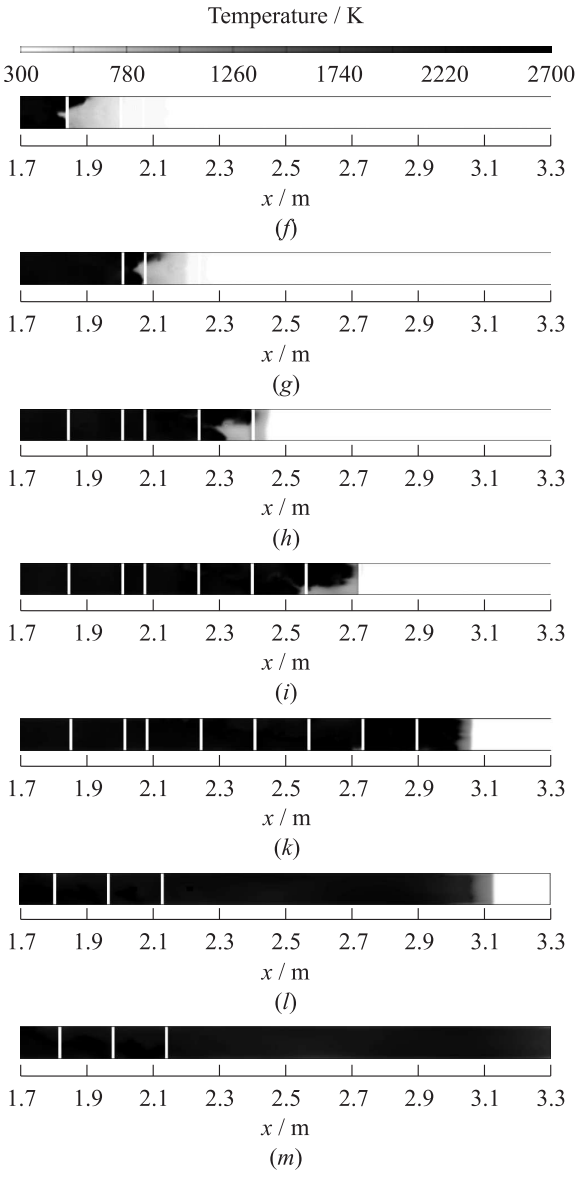

Figure 6 (*continued*) The calculated gas temperature field in the middle longitudinal section of the inner path of the PDE path at different time instants after prechamber ignition (check valve is closed): (*f*) 8 ms; (*j*) 8.25; (*h*) 8.5; (*i*) 8.75; (*j*) 9; (*k*) 9.25; (*l*) 9.5; and (*m*) 9.75 ms

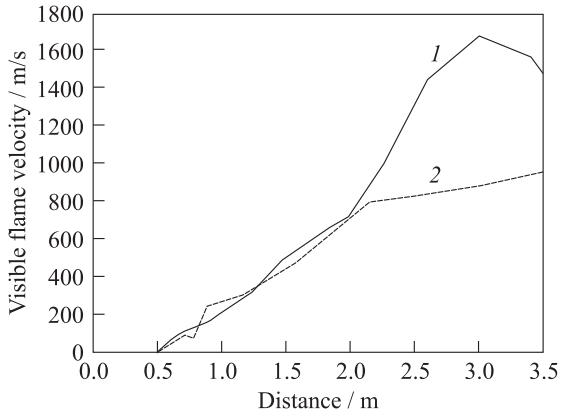

Figure 7 Comparison of calculated dependencies of the apparent flame front velocity on the traversed (axial) distance for two variants of the PDE: with DDT (*1*) and without DDT (*2*)

spatial distribution of fuel–air mixture in this example is the same as that shown in Fig. 5*a*.

Figure 7 compares the calculated dependencies of the visible flame front velocity on the traversed (axial) distance for two variants of the PDE: with and without DDT. In the first case, the turbulizing obstacles provide flame acceleration to 900–1000 m/s at the shortest distance (2.2–2.3 m), followed by a fast DDT [38] and the propagation of the detonation wave in the smooth section of the detonation tube. In the second case, the shape and arrangement of the turbulizing obstacles did not provide DDT. The decrease in the detonation velocity in the end section of the detonation tube is explained by the incomplete and inhomogeneous filling of the tube with the fresh fuel–air mixture (see Fig. 5*a*).

5 Concluding Remarks

Multivariant 3D calculations made it possible to design the PDE for an aircraft intended for the subsonic flight when operating on the polypropylene pyrolysis products. Since the pyrolysis products of polypropylene have detonability somewhat similar to the detonability of LPG in a stoichiometric mixture with air under normal conditions, the LPG–air mixture was used in the calculations. The PDE consists of an intake with a check valve, a fuel supply system, a prechamber ignition system, and a combustor with a detonation tube attached. Parametric 3D calculations allowed choosing the best length of the combustor, which provides an efficient mixing of air with fuel, the best way to ignite the mixture (prechamber-jet ignition), the best location of the prechamber, the minimum

length of the section with turbulizing obstacles for flame acceleration and DDT, and the best degree of filling the detonation tube with the fuel mixture to achieve the maximum completeness of combustion.

Acknowledgments

This work was supported by the Russian Foundation for Basic Research (Grant No. 18-08-00076a).

References

1. Zel'dovich, Ya. B. 1940. K voprosu ob energeticheskom ispol'zovanii detonatsionnogo goreniya [To the question of energy use of detonation combustion]. *Zh. Tekhn. Fiz.* [J. Tech. Phys.] 10(17):1455–1461.
2. Voitsekhovskii, B. V. 1959. Stationary detonation. *Dokl. Akad. Nauk SSSR* 129(6):1254–1256.
3. Bykovskii, F. A., and S. A. Zhdan. 2013. *Nepreryvnaya spinovaya detonatsiya* [Continuous spinning detonation]. Novosibirsk: SB RAS Publs. 423 p.
4. Frolov, S. M. 2006. *Impul'snye detonatsionnye dvigateli* [Pulsed detonation engines]. Moscow: TORUS PRESS. 592 p.
5. Frolov, S. M., V. S. Ivanov, I. O. Shamshin, and V. S. Aksenov. 2017. Ispytaniya modeli impul'sno-detonatsionnogo pryamotochnogo vozdushno-reaktivnogo dvigatelya v svobodnoy vozdushnoy strue s chislom Makha do 0.85 [Tests of the pulsed-detonation ramjet model in a free air jet with Mach number up to 0.85]. *Goren. Vzryv (Mosk.) — Combustion and Explosion* 10(3):43–52.
6. Canteins, G., F. Franzetti, R. Zitoun, D. Desbordes, and E. Daniau. 2003. PDE — possible ways for specific impulse improvement. *Confined detonations and pulse detonation engines*. Eds. G. Roy, S. Frolov, R. Santoro, and S. Tsyganov. Moscow: TORUS PRESS. 177–190.
7. Kailasanath, K. 2003. On the performance of pulse detonation engines. *Confined detonations and pulse detonation engines*. Eds. G. Roy, S. Frolov, R. Santoro, and S. Tsyganov. Moscow: TORUS PRESS. 191–202.
8. Frolov, S. M., V. I. Zvegintsev, V. S. Aksenov, I. V. Bilera, M. V. Kazachenko, I. O. Shamshin, P. A. Gusev, M. S. Belotserkovskaya, and E. V. Koverzanova. 2018. Detonatsionnaya sbosobnost' vozdushnykh smesey produktov piroliza polipropilena [Detonability of air mixtures of the polypropylene pyrolysis products]. *Goren. Vzryv (Mosk.) — Combustion and Explosion* 11(4):44–60. doi: 10.30826/CE18110406.
9. Brophy, C. M., D. W. Netzer, J. O. Sinibaldi, and R. G. Johnson. 2001. Detonation of a JP-10 aerosol for pulse detonation engine applications. *High-speed deflagration and detonation: Fundamentals and control*. Moscow: ELEX-KM Publs. 207–222.
10. Brophy, C. M., J. O. Sinibaldi, and P. Damphousse. 2002. Initiator performance for liquid-fueled pulse detonation engines. AIAA Paper No. 2002-0472.

11. Schauer, F. R., C. L. Miser, and K. C. Tucker. 2005. Detonation initiation of hydrocarbon–air mixtures in a pulsed detonation engine. AIAA Paper No. 2005-1343.
12. Frolov, S. M., and V. S. Aksenov. 2007. Deflagration-to-detonation transition in a kerosene–air mixture. *Dokl. Phys. Chem.* 416(Part 1):261–264.
13. Tang, H., Y. Huang, J. Li, and J. Wang. 2011. Deflagration-to-detonation transition of kerosene–air mixtures in a small-scale pulse detonation engine. *J. Aerospace Eng.* 225(G4):441–448.
14. Huang, Y., H. Tang, J. Li, and C. Zhang. 2012. Studies of DDT enhancement approaches for kerosene-fueled small-scale pulse detonation engines applications. *Shock Wave* 22(6):615–625.
15. Li, J.-M., C. J. Teo, P.-H. Chang, L. Li, K. S. Lim, and B. C. Khoo. 2017. Excessively fuel-rich conditions for cold starting of liquid-fuel pulse detonation engines. *J. Propul. Power* 33(1):71–79.
16. Borisov, A. A., B. E. Gelfand, S. A. Gubin, S. M. Kogarko, and A. L. Podgrebenkov. 1970. The reaction zone of two-phase detonations. *Astronaut. Acta* 15:411–419.
17. Zhdan, S. A. 1976. Calculation of spherical heterogeneous detonation. *Combust. Explo. Shock Waves* 12(4):586–594.
18. Zhdan, S. A. 1977. Calculation of heterogeneous detonation with regard for fuel drop deformation and breakup. *Combust. Explo. Shock Waves* 13(2):258–262.
19. Gubin, S. A., and M. Sichel. 1977. Calculation of the detonation velocity of liquid droplets and gaseous oxidizer. *Combust. Sci. Technol.* 17(3-4):109–117.
20. Eidelman, S., and A. Burkat. 1980. Evolution of a detonation wave in a cloud of fuel droplets. Part I: Influence of ignition explosion. *AIAA J.* 18(9):1103–1109.
21. Borisov, A. A., B. E. Gelfand, and A. V. Gubanov. 1981. The effect of relaxation processes on the detonation in heterogeneous mixtures. *Archivum Combustionis* 1(3/4):243–249.
22. Voronin, D. V., and S. A. Zhdan. 1984. Calculation of initiation of the heterogeneous detonation in tube by the explosion of hydrogen–oxygen mixture. *Combust. Explo. Shock Waves* 20(4):112–116.
23. Sichel, M. 1991. Numerical modeling of heterogeneous detonations. *Numerical approaches to combustion modeling.* Eds. E. S. Oran and J. P. Boris. Progress in astronautics and aeronautics science ser. New York, NY: AIAA Inc. 135:447–458.
24. Kailasanath, K. 2006. Liquid-fueled detonations in tubes. *J. Propul. Power* 22(6):1261–1268.
25. Frolov, S. M. 2009. *Detonations of liquid sprays and drop suspensions: Theory.* Von Karman Institute for Fluid Mechanics lecture ser. "Liquid fragmentation in high-speed flow." 36 p.
26. Frolov, S. M., and V. A. Smetanyuk. 2006. Teplo- i massoobmen kapli s gazovym potokom [Heat and mass transfer of liquid drop with gas flow]. *Khim. Fiz.* 25(4):42–54.
27. Ranz, W. E., and W. R. Marshall, Jr. 1952. Evaporation from drops, part I. *Chem. Eng. Prog.* 48:141–146

28. Borisov, A. A., S. M. Frolov, V. A. Smetanyuk, S. A. Polikhov, and C. Segal. 2005. Vzaimodeystvie kapli goryuchego s gazovym potokom [Interaction of fuel drop with gas flow]. *Khim. Fiz.* 24(7):50–57.
29. Yu, Y., and C. K. Law. 2002. Propagation and quenching of detonation waves in particle laden mixtures. *Combust. Flame* 129:356–364.
30. Lu, T. F., and C. K. Law. 2004. Heterogeneous effects in the propagation and quenching of heptane/air spray detonations. *J. Propul. Power* 20:820–827.
31. Zangiev, A. E., V. S. Ivanov, and S. M. Frolov. 2016. Thrust characteristics of an air-breathing pulse detonation engine in flight at Mach numbers of 0.4 to 5.0. *Russ. J. Phys. Chem. B* 10(2):272–283.
32. Reitz, R. D. Mechanism of atomization processes in high pressure vaporizing spray. 1987. *Atomization Spray Technology* 3:309–337.
33. Dukowicz, J. K. 1979. Quasi-steady droplet change in the presence of convection. Los Alamos Scientific Laboratory. Report LA7997-MS.
34. Basevich, V. Ya., and S. M. Frolov. 2006. Global'nye kineticheskie mekhanizmy dlya modelirovaniya mnogostadiynogo samovosplameneniya uglevodorodov v reagiruyushchikh techeniyakh [Overall kinetic mechanisms for modeling multistage self-ignition of hydrocarbons in reactive flows]. *Khim. Fiz.* 25(6):54–62.
35. Frolov, S. M., and V. S. Ivanov. 2010. Combined flame tracking – particle method for numerical simulation of deflagration-to-detonation transition. *Deflagrative and detonative combustion*. Eds. G. D. Roy and S. M. Frolov. Moscow: TORUS PRESS. 133–156.
36. Basevich, V. Ya., A. A. Belyaev, V. S. Posvyanskii, and S. M. Frolov. 2013. Mechanisms of the oxidation and combustion of normal paraffin hydrocarbons: Transition from C_1–C_{10} to C_{11}–C_{16}. *Russ. J. Phys. Chem. B* 7(2):161–169.
37. Frolov, S. M., V. S. Ivanov, B. Basara, and M. Suffa. 2013. Numerical simulation of flame propagation and localized preflame autoignition in enclosures. *J. Loss Prevent. Proc.* 26:302–309.
38. Frolov, S. M. 2008. Fast deflagration-to-detonation transition. *Russ. J. Phys. Chem. B* 2(3):442–455.

ЧИСЛЕННОЕ МОДЕЛИРОВАНИЕ ПЕРЕХОДА ГОРЕНИЯ В ДЕТОНАЦИЮ В ИМПУЛЬСНО-ДЕТОНАЦИОННОМ ДВИГАТЕЛЕ

А. Е. Зангиев[1], В. С. Иванов[1,3], С. М. Фролов[1,2,3]

[1]Федеральный исследовательский центр химической физики
им. Н. Н. Семёнова Российской академии наук
Россия, Москва
[2]Национальный исследовательский ядерный университет «МИФИ»
Россия, Москва
[3]Федеральное государственное учреждение «Федеральный научный центр
Научно-исследовательский институт системных исследований
Российской академии наук»
Россия, Москва

На основе аналитических оценок и параметрических многовариантных трехмерных (3D) расчетов разработан прототип воздушно-реактивного импульсно-детонационного двигателя (ИДД) для летательного аппарата, предназначенного для дозвукового полета при работе на продуктах пиролиза полипропилена. Прототип двигателя состоит из воздухозаборника с обратным клапаном, системы подачи топлива, форкамерной системы зажигания и камеры сгорания с присоединенной детонационной трубой. Параметрические 3D расчеты позволили выбрать оптимальную длину камеры сгорания ИДД, которая обеспечивает эффективное смешение воздуха с топливом, наилучший способ зажигания смеси (форкамерно-факельное), наилучшее расположение форкамеры, минимальную длину секции с турбулизирующими препятствиями для ускорения пламени и перехода горения в детонацию, а также наилучшую степень заполнения детонационной трубы топливной смесью для достижения максимальной полноты сгорания.